ISSN 0021-3640, JETP Letters, 2017, Vol. 106, No. 7, pp. 460–464. © Pleiades Publishing, Inc., 2017.
Original Russian Text © D.P. Pavlov, I.I. Piyanzina, V.M. Mukhortov, A.M. Balbashov, D.A. Tayurskii, I.A. Garifullin, R.F. Mamin, 2017, published in Pis'ma v Zhurnal Eksperimental'noi i Teoreticheskoi Fiziki, 2017, Vol. 106, No. 7, pp. 440–444.

CONDENSED MATTER

Two-Dimensional Electron Gas at the Interface of $Ba_{0.8}Sr_{0.2}TiO_3$ Ferroelectric and $LaMnO_3$ Antiferromagnet

D. P. Pavlov[a], I. I. Piyanzina[a, b], V. M. Mukhortov[c], A. M. Balbashov[d], D. A. Tayurskii[b], I. A. Garifullin[a], and R. F. Mamin[a, b, *]

[a] *Zavoisky Physical-Technical Institute, Kazan Scientific Center, Russian Academy of Sciences, Kazan, 420029 Russia*
[b] *Kazan Federal University, Kazan, 420008 Russia*
[c] *Southern Scientific Center, Russian Academy of Sciences, Rostov-on-Don, 344006 Russia*
[d] *Moscow Power Engineering Institute, Moscow, 111250 Russia*
**e-mail: mamin@kfti.knc.ru*

Received September 6, 2017

The temperature dependence of the electrical resistance has been studied for heterostructures formed by antiferromagnetic $LaMnO_3$ single crystals of different orientations with epitaxial films of ferroelectric $Ba_{0.8}Sr_{0.2}TiO_3$ deposited onto them. The measured electrical resistance is compared to that exhibited by $LaMnO_3$ single crystals without the films. It is found that, in the samples with the film, for which the axis of polarization in the ferroelectric is directed along the perpendicular to the surface of the single crystal, the electrical resistance decreases significantly with temperature, exhibiting metallic behavior below 160 K. The numerical simulations of the structural and electronic characteristics of the $BaTiO_3/LaMnO_3$ ferroelectric–antiferromagnet heterostructure has been performed. The transition to the state with two-dimensional electron gas at the interface is demonstrated.

DOI: 10.1134/S0021364017190109

A high-mobility electron gas was first observed in 2004 [1] at the interface between $LaAlO_3$ (LAO) and $SrTiO_3$ (STO). After that, such heterointerfaces involving two insulating and nonmagnetic oxides were comprehensively studied. In particular, it was found that the nanometer-thick metallic phase (two-dimensional electron gas, 2DEG) is formed in the STO layers at the LAO/STO interface when the number of $LaAlO_2$ layers is larger than three [2]. Such a system undergoes a transition to a superconducting state at temperatures below 300 mK [3]. The charge carrier density in this heterostructure is as high as 3×10^{13} cm^{-2}. In addition, the LAO/STO heterostructure exhibits ferromagnetism [4]. Later on, the two-dimensional electron gas was revealed at interfaces between other nonmagnetic insulators, e.g., $KTaO_3/SrTiO_3$ [5] and $CaZrO_3/SrTiO_3$ [6]. The 2DEG was also found at the interfaces between magnetically ordered Mott insulators and, in particular, ferromagnetic $GdTiO_3$ (GTO) [7], antiferromagnetic $SmTiO_3$ [8] and $LaTiO_3$ [9], having the highest possible charge carrier density equal to 3×10^{14} cm^{-2}. Further on, the 2DEG formation was demonstrated also in $NdAlO_3/SrTiO_3$, $PrAlO_3/SrTiO_3$, and $NdGaO_3/SrTiO_3$ heterostructures [10], as well as in $LaGaO_3/SrTiO_3$ [11].

It is supposed that the conductivity arises owing to the structural and hence electronic reconstruction. However, firmly established mechanisms and commonly accepted models for the arising conductivity are still missing. It is usually assumed that the local polarity of $(LaO)^{+1}$ and $(AlO_2)^{-1}$ layers in LAO plays an important role in the formation of 2DEG. Having this in mind, we choose the heterostructure of the $BaTiO_3/LaMnO_3$ (BTO/LMO) type for our study of the relation of the structural distortions, electronic reconstruction, and the polar characteristics. This heterostructure exhibits the ferroelectric polarization related to the shift of Ti^{+4} atoms from the symmetry center of the oxygen octahedron in BTO, in spite of the electric neutrality of the BaO and TiO_2 layers. The direction of such polarization can be switched by the applied electric field. Note that it is not possible to perform the switching in LAO, since the $(LaO)^{+1}$ and $(AlO_2)^{-1}$ layers cannot interchange their positions under effect of some external field. In addition, the BTO/LMO heterostructure is interesting because $LaMnO_3$ does not exhibit the ferromagnetic order, being an antiferromagnet. There is a tempting idea to transform $LaMnO_3$ to the ferromagnetic state by an increase in the density of itinerant charge carriers [12], because this leads to the enhancement of the indirect ferromagnetic exchange interaction. This is actually

implemented by doping of LMO [12, 13]. In other words, we can expect in the future that an increase in the number of charge carriers at the interface is apt to give rise to the local ferromagnetic state and to the formation of the magnetoresistive characteristics [13] in such system with 2DEG. Thus, in the BTO/LMO heterostructure, both the conductivity (the trigger effect) and magnetization (magnetoelectric effect) can be switched by an electric field, and in addition the transport characteristics can be changed by an applied magnetic field (magnetoresistive effect). In this paper, we also present the results of numerical simulations of the $BaTiO_3/LaMnO_3$ (BTO/LMO) system and the results of the studies of the electrical conductivity for the $Ba_{0.8}Sr_{0.2}TiO_3/LaMnO_3$ (BSTO/LMO) heterostructure having a BSTO layer 350 nm thick.

In our experiments, we used LMO single crystals, onto the modified surface of which epitaxial BSTO films had been deposited by magnetron sputtering. The choice of these objects was primarily justified by the well-developed technologies used in the preparation of each individual constituent [14–16]. Note that BSTO with the Sr content equal to 0.2 only slightly differs from BTO, and the ferroelectric transition temperature T_c for the films is rather high: for 300-nm-thick films, we have $T_c \sim 540$ K [15]. We used 350-nm-thick films because, generally, the properties of 2DEG do not change much beginning from a certain thickness of the part of the system which exhibits the polar characteristics. The results of our numerical simulations support this statement. In this work, it was important to find the effect itself and to fix it reliably, whereas the role of the ferroelectric layer thickness in the formation of the 2DEG characteristics should be an object of future studies. We grew single crystals of $LaMnO_3$ manganite, onto which $Ba_{0.8}Sr_{0.2}TiO_3$ (BSTO) was deposited, and the conductivity of this system was measured by the four-probe technique. Simultaneously, we began the numerical simulations of the structural and electron characteristics of the BTO/LMO heterostructure.

First, we present the results obtained by the computer simulation of the characteristics of the BTO/LMO heterostructure. As the numerical technique, we use the density functional theory [17]. The exchange and correlation effects were taken into account in the framework of the generalized gradient approximation (GGA) [18]. The Kohn–Sham equations were solved using the projector augmented wave (PAW) basis [19] implemented in the VASP code [20] integrated into the MedeA software program [21]. The energy cutoff was chosen to be equal to 400 eV, the force tolerance was taken to be 0.05 eV, and the energy tolerance for the self-consistency loop was 10^{-5} eV. The Brillouin zone is divided using a $5 \times 5 \times 1$ grid. In the numerical simulations of the electronic properties of transition metal oxides, it is necessary to take into account strong correlations between electrons belonging to d and f orbitals; therefore, we chose the GGA + U method with the corrections introduced according to the procedure discussed in [23]. The parameter U was added for La 4f, Ti 3d, and Mn 4d (U = 8 eV, 2 eV, and 4 eV, respectively). The magnetic nature of this material was taken into account.

In Fig. 1a, we illustrate the structure of half of the unit cell for the LMO/BTO heterostructure with the BaO layer at the interface. For bulk orthorhombic $LaMnO_3$, the lattice constants are $a = 5.650$ Å, $b = 5.616$ Å, and $c = 7.935$ Å. These values were obtained after optimization (for comparison, the experiment gives $a = 5.537$ Å, $b = 5.749$ Å, $c = 7.665$ Å). In order to perform the numerical simulations of the heterostructure, the LMO unit cell was expanded by a factor of 1.5 and surrounded from both sides by a variable number of $BaTiO_3$ layers with BaO layers at the interface and TiO_2 layers at the surface and vice versa. The second half of the unit cell shown in Fig. 1a is the mirror reflection with respect to the central LaO layer. Such form of the structure ensures the absence of polarity and the dipole moment arising owing to an asymmetry of the unit cell. To avoid an undesirable interaction of the surfaces with their periodic copies, we added to the system a vacuum spacer ≈20 Å thick located in the direction perpendicular to the interface. To imitate the "rigidity" of the LMO substrate, we fixed the a and b lattice parameters, whereas the atomic positions can vary in the process of the heterostructure optimization.

In the course of the optimization of both types of interface (the first and second cases with the BaO interface layer and the TiO_2 layer, respectively), it is found that, in the latter case, the energy is lower; i.e., the structure is more stable. Having this in mind, in all further discussions, we deal just with this case. In Fig. 1a, we can see that, in the near-surface TiO_2 layer, Ti atoms come out from the oxygen layer by about 0.15 Å. This gives rise to the dipole moment directed toward the interface. To get a better insight into the character of structural distortions, the calculations involving a larger number of BTO layers are under way.

To determine the electronic characteristics of the structure, we calculated the spectrum of the density of states taking into account the magnetic properties of LMO. In Fig. 1b, we present the results of such calculation separately for Mn, La, and Ti atoms involved in such structure. We can see that, even for a single BTO layer, the gap is closed and the energy levels corresponding to Mn cross the Fermi level. The total magnetization arises as well, being located mostly at Mn atoms.

The measurements has been performed with three types of samples: (i) samples N1 are LMO single crystals with BSTO film deposited onto the surface, within the plane of which lies the c axis of the single crystal; (ii) samples N2 are LMO single crystals with BSTO

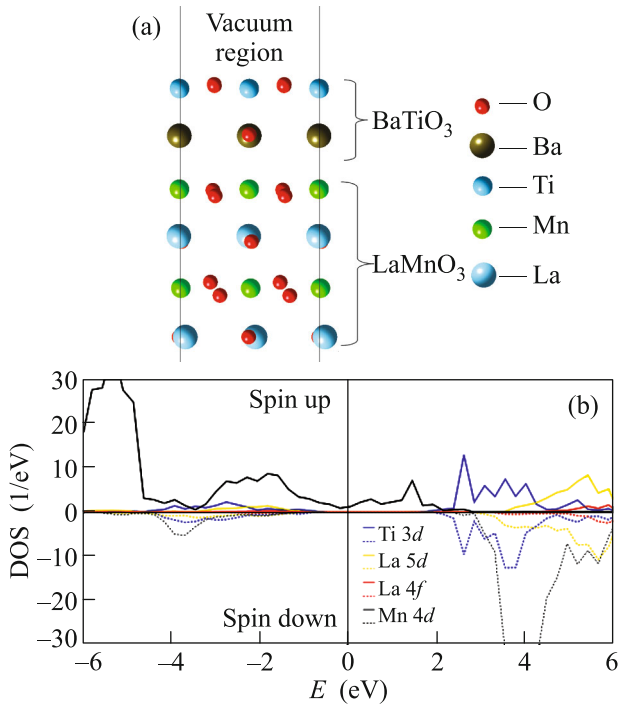

Fig. 1. (Color online) (a) Structure of the half unit cell of the LMO/BTO heterostructure with the BaO interface layer. (b) Density of states spectrum of the LMO/BTO heterostructure with the BaO interface layer.

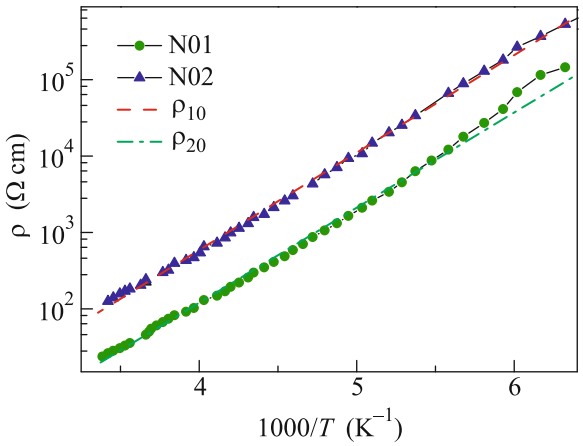

Fig. 2. (Color online) Temperature dependence of the electrical resistivity $\rho(T)$ for $LaMnO_3$.

film deposited onto the surface, where the atomic plane is perpendicular to the c axis of the single crystal; and (iii) samples N01 and N02 are LMO single crystals similar to those in samples N1 and N2 but without the film. The X-ray diffraction studies demonstrated that, for the N1 samples, the c axis of the film, along which the spontaneous polarization of ferroelectric is directed, lies within the film plane, whereas for the N2 samples, the c axis of the film is perpendicular to the film plane. Such an arrangement stems from the fact that, in the first case, the LMO substrate is a stretching one with respect to the film, while in the second case, the substrate compresses the film [16]. In both cases, this is due to the ratio of the unit cell sizes of the single crystal and the film. In Fig. 2, we illustrate the results of four-probe measurements of the electrical resistivity $\rho(T)$ performed using the N01 and N02 samples with the electric current directed perpendicular to the c axis. We see that the resistivity exhibits the activation-type behavior characteristic of the conductivity in semiconductors. It corresponds to the behavior of conductivity in LMO measured on similar samples [13, 14]. Performing the numerical analysis of the resistivity according the formulas $\rho_{10}(T) = \rho_{01}\exp(T_{a1}/T)$, $\rho_{20}(T) = \rho_{02}\times\exp(T_{a2}/T)$ (the results are shown in Fig. 2 by the red dashed and green dot-dash lines for the orientations of the plane perpendicular and parallel to the c axis, respectively), we obtain the following values: $\rho_{01} = 4.64\times10^{-3}$ Ω cm, $T_{a1} = 2938$ K and $\rho_{02} = 1.25\times10^{-3}$ Ω cm, $T_{a2} = 2869$ K.

In Fig. 3, we illustrate the results of four-probe measurements of the electrical resistance performed using the N1 sample in the configuration with the c axis of LMO single crystals directed perpendicular to the electric current. We can see that the resistivity exhibits the activation-type behavior within the whole temperature range of the measurements. In Fig. 4, we illustrate the results of electrical resistance measurements performed using the N2 sample. Since the c axis of the LMO single crystals is directed perpendicular to the film plane, the current flows in the direction perpendicular to the c axis. At high temperatures, the electrical resistance of N2 sample behaves in an activation-like way, whereas at temperatures below 160 K, it passes to the regime characteristic of the metallic-type behavior. The total electrical resistance of the N2 sample is several times lower than the electrical resistance R_0, which the sample would exhibit without the film (in Fig. 4, it is shown by the dashed line obtained on the basis of the resistivity data illustrated in Fig. 2), within the whole temperature range of the measurements. In our opinion, the drastic decrease in the electrical resistance at low temperatures is a signature of the transition to the state with 2DEG.

Let us analyze the results and make some estimates for the parameters characterizing the arising state. We assume that the electric current flows along three layers with different conducting characteristics: the single-crystalline LMO layer with the electrical resistance R_0 (shown by the dashed line in Fig. 4); the ferroelectric layer with a very high resistance (where the current nearly vanishes); and the layer with a high charge carrier density at the interface, i.e., the near-surface region in LMO with the characteristic size Δ.

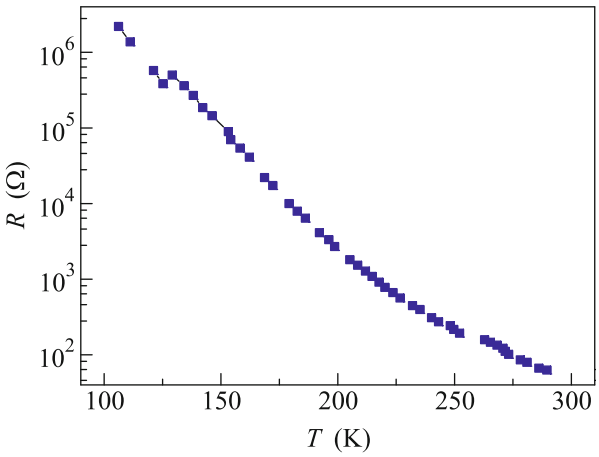

Fig. 3. (Color online) Temperature dependence of the electrical resistance $R(T)$ for sample N1 with the $Ba_{0.8}Sr_{0.2}TiO_3/LaMnO_3$ heterostructure having the 350-nm-thick $Ba_{0.8}Sr_{0.2}TiO_3$ layer.

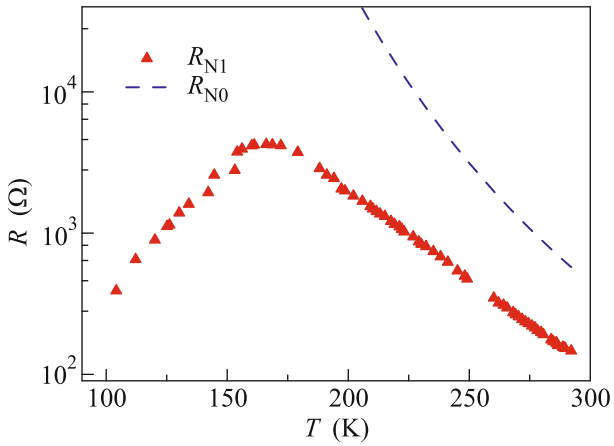

Fig. 4. (Color online) Temperature dependence of the electrical resistance $R(T)$ for sample N2 with the $Ba_{0.8}Sr_{0.2}TiO_3/LaMnO_3$ heterostructure having the 350-nm-thick $Ba_{0.8}Sr_{0.2}TiO_3$ layer. The dashed line shows the temperature dependence of the electrical resistance for the similar $LaMnO_3$ sample without the film.

The electrical resistance of the latter layer is R_S. Then, the electrical resistance R_S can be determined using the formula $R_S = R_0R/(R_0 - R)$, where R is the measured electrical resistance of the sample. Near the temperature of liquid nitrogen, we have $R_S \approx R \approx 200$ Ω. Now, let us take into account that R_S can be expressed in the form

$$R_S = \frac{\rho_m l}{d\Delta}, \quad (1)$$

where ρ_m is the electrical resistivity of manganite in the metallic state, l is the length of the section across which the resistance is measured (the distance between the voltage contacts, $l = 0.14$ cm), and d is the transverse size of the area of the resistance measurements ($d = 0.33$ cm).

For the surface charge carrier density, we can write $n_s = n_v\Delta$, where n_v is the charge carrier density in the bulk. Then, taking (1) into account, we find

$$n_s = \frac{\rho_m n_v l}{R_S d}. \quad (2)$$

The number of charge carriers per unit cell (doping level) is of the order of $x_0 = 0.175$–0.3, which is characteristic of lanthanum manganites with the metallic type of conductivity at low temperatures. We can write $n_v = x_0(abc)^{-1}$ (a, b, and c are the unit cell parameters for LMO). Then, using the known values $\rho_m = 6\times10^{-5}$–2×10^{-4} Ω cm for the electrical resistivity near the liquid nitrogen temperature for manganites, which have the chemical composition corresponding to the same charge carrier density [14], we obtain the surface charge carrier density $n_s = (1.65$–$3.03)\times10^{14}$ cm^{-2}. As a result, we have the following estimates for thickness $\Delta = n_s n_v^{-1}$ of the layer where the high-mobility electron gas is formed: $\Delta \approx (1.65$–$5.51)c_e = 1.265$–4.216 nm (here, $c_e = 7.665$ Å is the LMO unit cell size in the direction of the c axis).

Note in conclusion that the deposition procedures for BSTO films are optimized to such an extent that the doping of substrates by the chemical elements forming the films does not occur [15, 16]. Therefore, we can be sure that the observed effects are not related to the implantation of spurious atoms, e.g. Sr, to the near-surface layers of LMO single crystal. An indirect indication of this is the observation of the high-mobility electron gas at one LMO orientation (N2 samples) and the absence of such observation at another orientation (N1 samples). The manifestations of magnetic properties of the BSTO/LMO, the effect of applied magnetic field on the 2DEG conductivity in this heterostructure, and the role of ferroelectric layer thickness on the characteristics of 2DEG will be discussed elsewhere.

Thus, in this work, we have performed the numerical simulation of the structural and electronic properties of the $BaTiO_3/LaMnO_3$ ferroelectric–antiferromagnet heterostructure. The role of structural reconstruction in the formation of the interfacial metallic state is revealed. The electrical resistance of the antiferromagnetic single-crystalline $LaMnO_3$ sample has been measured. After that, the magnetron sputtering technique has been used for the deposition of $Ba_{0.8}Sr_{0.2}TiO_3$ films onto these samples. The study of electrical conductivity of these samples shows that, in the samples with films, the electrical resistance drastically decreases and, at temperatures below 160 K, transitions to the metallic type in the case where the

ferroelectric polarization axis is directed perpendicular to the surface of the single crystal. This corresponds to the case where the film is deposited onto the surface perpendicular to the c axis of $LaMnO_3$ single crystal and the substrate turns out to be a compressing one with respect to the film.

We are grateful to Yu.I. Golovko for the assistance in the characterization of the sample and to S.A. Migachev for the preparation of the single crystals to make them ready for the film deposition. The authors from Kazan Federal University acknowledge partial support by the Program of Competitive Growth of Kazan Federal University. This study was supported by the Supercomputing Center, Moscow State University.

REFERENCES

1. A. Ohtomo and H. Y. Hwang, Nature **427**, 423 (2004); Nat. Mater. **5**, 204 (2006).
2. S. Thiel, G. Hammerl, A. Schmehl, C. W. Schneider, and J. Mannhart, Science **313**, 1942 (2006).
3. N. Reyren, S. Thiel, A. D. Caviglia, L. Fitting Kourkoutis, G. Hammerl, C. Richter, C. W. Schneider, T. Kopp, A.-S. Rüetschi, D. Jaccard, M. Gabay, D. A. Muller, J.-M. Triscone, and J. Mannhart, Science **317**, 1196 (2007).
4. A. Brinkman, M. Huijben, M. Van Zalk, J. Huijben, U. Zeitler, J. C. Maan, W. G. van der Wiel, G. Rijnders, D. H. A. Blank, and H. Hilgenkamp, Nat. Mater. **6**, 493 (2007).
5. A. Kalabukhov, R. Gunnarsson, J. Börjesson, E. Olsson, T. Claeson, and D. Winkler, Phys. Rev. B **75**, 121404 (2007).
6. W. Chen, L. Li, J. Qi, Y. Wang, and Z. Gui, J. Am. Ceram. Soc. **81**, 2751 (1998).
7. P. Moetakef, T. A. Cain, D. G. Ouellette, J. Y. Zhang, D. O. Klenov, A. Janotti, Ch. G. van de Walle, S. Rajan, S. J. Allen, and S. Stemmer, Appl. Phys. Lett. **99**, 232116 (2011).
8. C. A. Jackson and S. Stemmer, Phys. Rev. B **88**, 180403 (2013).
9. J. Biscaras, N. Bergeal, A. Kushwaha, T. Wolf, A. Rastogi, R. C. Budhani, and J. Lesueur, Nat. Commun. **1**, 89 (2010).
10. A. Annadi, A. Putra, Z. Q. Liu, X. Wang, K. Gopinadhan, Z. Huang, S. Dhar, T. Venkatesan, and Ariando, Phys. Rev. B **86**, 085450 (2012).
11. P. Perna, D. Maccariello, M. Radovic, U. Scotti di Uccio, I. Pallecchi, M. Codda, D. Marré, C. Cantoni, M. Varela, S. J. Pennycook, and F. M. Granozio, Appl. Phys. Lett. **97**, 152111 (2010).
12. P.-G. de Gennes, Phys. Rev. **118**, 141 (1960).
13. E. Dagotto, T. Hotta, and A. Moreo, Phys. Rep. **344**, 1 (2001).
14. A. A. Mukhin, V. Yu. Ivanov, V. D. Travkin, S. P. Lebedev, A. Pimenov, A. Loidl, and A. M. Balbashov, JETP Lett. **68**, 356 (1998).
15. Yu. I. Golovko, V. M. Mukhortov, Yu. I. Yuzyuk, P. E. Janolin, and B. Dkhil, Phys. Solid State **50**, 485 (2008).
16. A. S. Sigov, E. D. Mishina, and V. M. Mukhortov, Phys. Solid State **52**, 762 (2010).
17. P. Hohenberg and W. Kohn, Phys. Rev. B **136**, 864 (1964).
18. J. P. Perdew, K. Burke, and M. Ernzerhof, Phys. Rev. Lett. **77**, 3865 (1996).
19. MedeAAM-2.20 (Materials Design, Inc., San Diego, CA, 2015).
20. G. Kresse and J. Furthmüller, Comput. Mater. Sci. **6**, 15 (1996).
21. I. I. Piyanzina, T. Kopp, Yu. V. Lysogosrkiy, D. Tayurskii, and V. Eyert, J. Phys.: Condens. Matter **29**, 095501 (2017).
22. J. Rodriguez-Carvajal, M. Hennion, F. Moussa, A. H. Moudden, L. Pinsard, and A. Revcolevschi, Phys. Rev. B **57**, R3189 (1998).
23. S. L. Dudarev, G. A. Botton, S. Y. Savrasov, C. J. Humphreys, and A. P. Sutton, Phys. Rev. B **57**, 1505 (1998).

Translated by K. Kugel